*Kovove Mater. 50 2012 59–67*
*DOI: 10.4149/km_2012_1_59*



# Determination of solidification sequence of the AlMg9 alloy

Z. Zovko Brodarac[1*], F. Unkić[1], J. Medved[2], P. Mrvar[2]

[1] *Faculty of Metallurgy, University of Zagreb, Aleja narodnih heroja 3, 44103 Sisak, Republic of Croatia*
[2] *Faculty of Natural Science and Engineering, University of Ljubljana, Department for the Materials and Metallurgy, Aškerčeva c. 12, 1000 Ljubljana, Republic of Slovenia*

Received 18 January 2011, received in revised form 22 April 2011, accepted 28 April 2011

**Abstract**

Foundry Al-Mg alloys play an important role in overall foundry industry of light metals due to their outstanding properties, although their solidification mechanism has not been clearly determined. Solidification overview of multicomponent technical AlMg9 alloy was obtained in this work. One of significant achievement was application of "disturbed" solidification method by quenching at exactly determined temperature to obtain frozen microstructure. This method enables correlation between characteristic temperatures of phase transformations and corresponding characteristics of microstructure constituent. Mathematical expression related to the quenching temperature and time enable prediction of microstructure development during solidification of AlMg9 alloy. Chemical composition determination of particular phases, carried out by energy dispersive spectroscopy (EDS), resulted in identification of $Al_x(MnFe)_ySi_z$, $Mg_2Si$ and $Al_8Mg_5$ phases. Temperature and time solidification sequence were determined and compared to the predicted ones, by phase diagram modeling. The change of particular phase ratio during solidification process was established also by mathematical modeling. These models offer an oversight of the required solidification microstructure development.

K e y w o r d s: Al-Mg alloy, solidification, quenching, simultaneous thermal analysis, microstructure development

## 1. Introduction

Aluminum alloy castings are being used increasingly during the last few decades together with the tendency of industry to establish new ways for downsizing and properties improving. The quality factor is based on the development and application of new compounds, alloys as well as numerous methods of investigation of their properties [1–4].

Recently, more attractive became cast alloys on the base of aluminum-magnesium system due to low density, from which follows the reducing of the casting weight, as well as suitability for recycling. Maximum solubility of magnesium in aluminum is 17.4 mass % at the eutectic temperature of 449 °C, which provides a wide range of compositions with different physical and mechanical properties [5]. Subsequently the cast alloys have been chosen from $\alpha$-phase region. Aluminum and magnesium form an intermetallic compound $Al_8Mg_5$, ($\beta$-phase), earlier known as $Al_3Mg_2$ [6–9], which is very hard and brittle and hardly takes shape through the plastic deformation and evaluates below the eutectic temperature [10, 11], and does not have any influence on strengthening due to precipitation as the coarse particles on grain boundaries. Due to high mass content of magnesium this phase first crosses into the solution. This is the reason for ternary system development.

The most common ternary alloy composition is one on the base of Al-Mg-Si system, which is strengthened by the precipitation of metastable compound $Mg_2Si$. Surface tension of ternary alloy is decreased with the magnesium and silicon addition [7]. Magnesium expands the crystal lattice of aluminum, and silicon tries to shrink it, so the real lattice parameter of the aluminum together with magnesium and silicon in solution is less than those calculated by the total addition of magnesium and silicon [7]. In non-equilibrium

*Corresponding author: tel.: 00385 44 533 379; fax: 00385 44 533 378; e-mail address: zovko@simet.hr

Table 1. Invariant five – phase reactions at aluminum corner of the Al-Fe-Mg-Si and Al-Fe-Mn-Si systems [9]

| Reactions | $T$ (°C) | Composition of the liquid | | |
|---|---|---|---|---|
| | | Fe (mass %) | Mg or Mn (mass %) | Si (mass %) |
| $L + Al_3Fe + Al_6(Fe,Mn) \rightarrow \alpha_{Al} + Al_{15}(Fe,Mn)_3Si_2$ | 648 | 2.0 | 0.35 | 1.75 |
| $L + Al_3Fe \rightarrow \alpha_{Al} + Al_8Fe_2Si + Al_{15}(Fe,Mn)_3Si_2$ | 627–632 | 2–2.5 | $< 0.2$ | 3–5 |
| $L + Al_8Fe_2Si \rightarrow \alpha_{Al} + Al_5FeSi + Al_{15}(Fe,Mn)_3Si_2$ | 597–607 | 1–2 | 0.1–0.5 | 5–10 |
| $L \rightarrow \alpha_{Al} + Mg_2Si$ | $> 587$ | $\sim 1.0$ | $\sim 10.0$ | $\sim 7.0$ |
| $L \rightarrow \alpha_{Al} + (Si) + Mg_2Si + Al_8FeMg_3Si_6$ | 554 | 0.15 | 4.9 | 12.9 |
| $L \rightarrow \alpha_{Al} + Al_3Fe + Al_8Mg_5 + Mg_2Si$ | 448 | 0.11 | 33.3 | 0.35 |

condition such as rapid cooling, the tendency to the local segregation is present, at which all of silicon is evaluated as $Mg_2Si$ phase [7]. At high content of magnesium, only $Mg_2Si$ is present, while low magnesium content favors silicon evolution as a secondary phase particle [12]. Due to the dendrite segregation in alloys which are in equilibrium conditions monophased, $Mg_2Si$ or $Al_8Mg_5$ could appear.

Since most of commercial alloys contain small amount of iron and manganese that can act as impurities, alloying element system must be observed as Al-Fe-Mg-Si and respectively Al-Fe-Mn-Si systems. Invariant five-phase reactions occurred in alloys from those systems are listed in Table 1 [7].

According to invariant reactions in investigated Al-Fe-Mg-Si and Al-Fe-Mn-Si systems three main groups of reaction are indicated: evolution of Fe-rich intermetallic phases, precipitation of co-eutectic phase $Mg_2Si$, and finally precipitation of the secondary co-eutectic $Al_8Mg_5$ phase [9].

Literature overview and phase diagram modeling enable the presuming of solidification sequence of multicomponent technical AlMg9 alloy. Solidification of the AlMg9 alloy was investigated by simultaneous thermal analysis and microstructure examination of fast cooled samples. Correlation of thermal analysis results and microstructural constituent's characteristics enable establishing the solidification sequence.

## 2. Experimental

Thermodynamic calculation of phase equilibrium of multicomponent technical AlMg9 alloy (EN 51200, [13]) was provided by the software ThermoCalc (TCW 4). Thermodynamic calculation resulted in construction of equilibrium phase diagram from which all thermodynamically stable phases and their temperature stability intervals could be calculated in relation to the determined thermodynamic conditions.

The charge material for casting process were ingots of EN 51200 quality. An alloy was melted in induction furnace. Melt was cast at pouring temperature of 730 °C from the graphite pot into the measuring cell made by cronning cell (standard Quick Cup equipped by thermoelement Ni-CrNi).

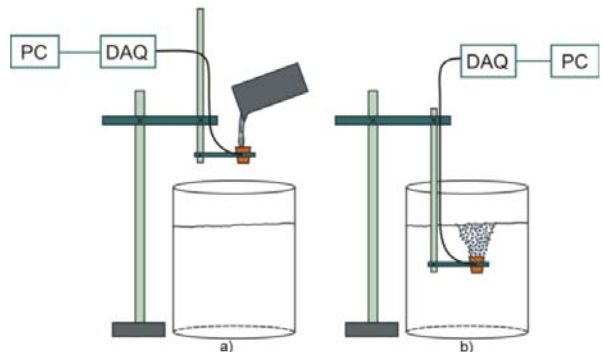


Fig. 1a,b. Schematic representation of the "disturbed" solidification by quenching.

Solidification sequence was determined using "disturbed" solidification process. "Disturbed" solidification was performed by quenching of samples in water to achieve frozen microstructure at exact temperatures chosen on the base of cooling and solidification curve in order to cover entire solidification area. Figure 1 schematically represents the methodology of "disturbed" solidification by quenching experiment. Figure 1a shows the melt poured into the cronning cell before diving into the water, while Fig. 1b illustrates the quenching process.

The solidification sequence of the examined AlMg9 alloy was interpreted by the microstructural analyses of the samples with frozen microstructure. Cronning cell, in which all of samples were poured, is shown in Fig. 2a. From obtained cast samples, specimens for the metallographic examinations were taken from exactly determined places on which the thermoelements were placed, as shown in Figs. 2b,c.

Samples for optical metallographic and microstructural investigations were prepared by standard procedure of grinding and polishing and afterwards etching in diluted HF. Microstructural analysis was performed on Olympus BX61 optical microscope

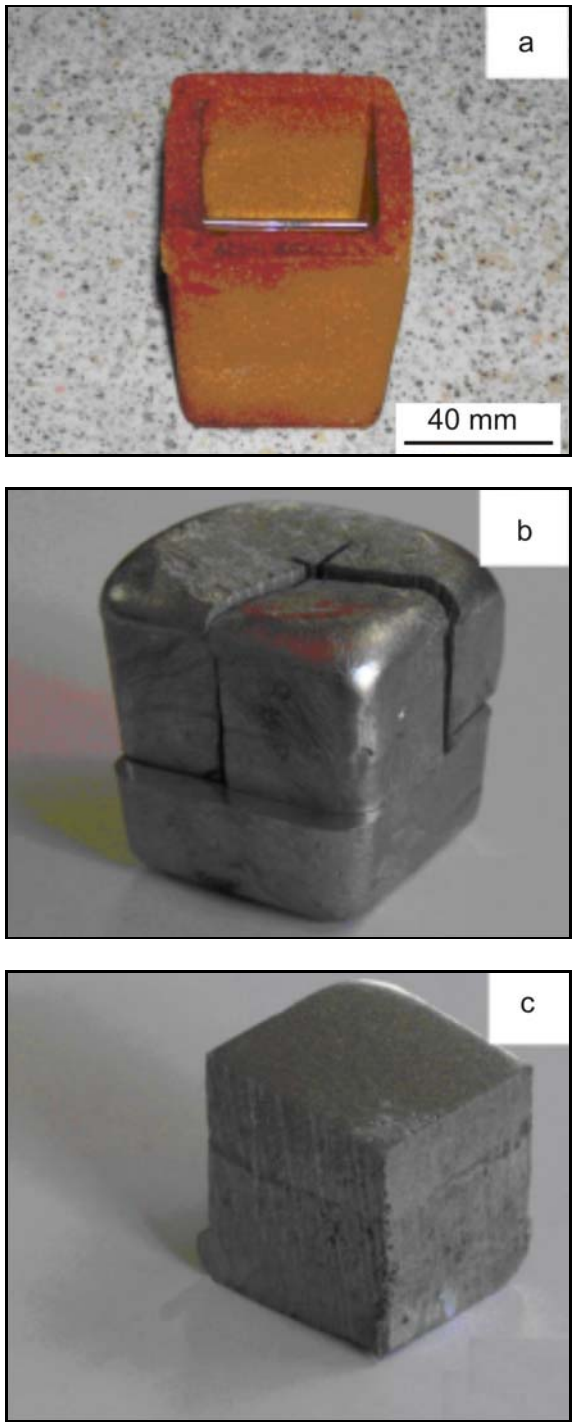


Fig. 2. Cast equipment and samples: a) measuring cell (Quick Cup), b) cast sample, c) sample for metallographic examination.

equipped by automatic image analysis by the software Analysis®MaterialsResearchLab. Metallographic analysis includes phase ratio as well as particles area and elongation. Samples for the microstructural investigations were also examined on the scanning electron microscope (SEM) JEOL 5610 with the phase recognition on the base of chemical composition analysis by the energy dispersive spectrometer (EDS). Samples for grain size determination were also undergone the standard procedure of preparation along with the electrolytic etching by voltage of 23 V in Barker reagent during 40 s.

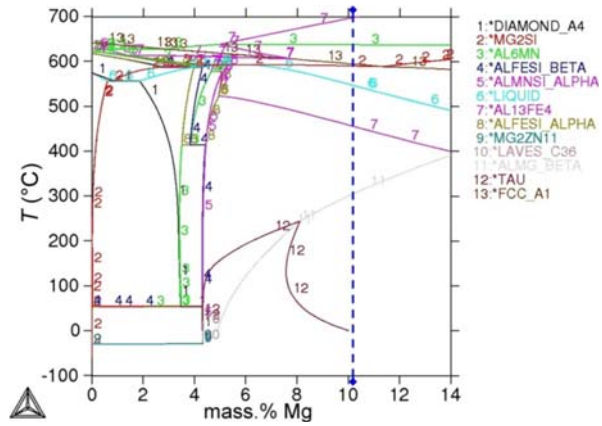


Fig. 3. Polythermic section of equilibrium phase diagram of examined AlMg9 alloy obtained by thermodynamic calculation.

Simultaneous thermal analysis (STA) has been performed by the method of differential scanning calorimetry (DSC) by the instrument Netzsch STA 449C Jupiter on the marked sample, by the technique of heating and cooling in order to establish corresponding significant temperatures of the phase transformations and solidification intervals, as well as corresponding enthalpies of particular phases. This analysis was related to lowest cooling rate of 0.17 K $s^{-1}$.

Established temperatures of phase changes were afterwards correlated by mathematical modeling to the determined phase ratio in order to provide temperature and time solidification sequence of the AlMg9 alloy.

## 3. Results and discussion

### *3.1. Chemical composition analysis*

Chemical composition of the cast samples, examined by flame spectrometer, is given in Table 2.

Chemical composition shows no deviations from reference values prescribed by norm EN 1706:1998 [13].

Thermodynamic calculation of particular phases by initial condition of temperature 743 ℃, pressure $10^8$ kPa and default chemical composition resulted in phase diagram of evolution in Fig. 3.

The magnesium concentration of 10.08 mass % in examined alloy is marked on the diagram. Thermodynamic calculation of the equilibrium stability of par-

Table 2. Chemical composition of examined multicomponent technical AlMg9 alloy

| Element | Si | Fe | Cu | Mn | Mg | Cr | Ni | Zn | Ti |
|---|---|---|---|---|---|---|---|---|---|
| $w$ (mass %) | 1.212 | 0.757 | 0.0543 | 0.2966 | 10.08 | 0.0034 | 0.0086 | 0.0231 | 0.0904 |

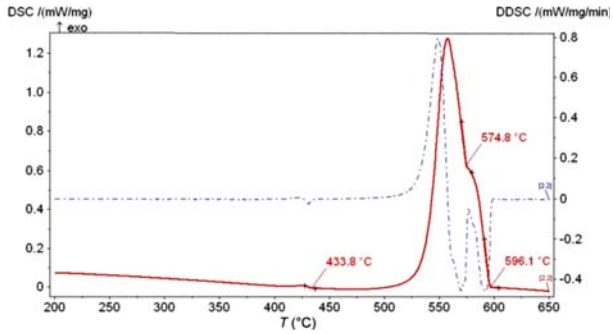


Fig. 4. Cooling curve obtained by simultaneous thermal analysis of AlMg9 alloy.

ticular phases by ThermoCalc resulted in presumed solidification sequence: iron reached phase $Al_{13}Fe_4$ at 703 ℃; $Al_6Mn$ phase was stable below 617 ℃; evolution of $\alpha_{Al}$ and development of the dendrite network comprehended to the liquidus temperature $T_L$ = 597.3 ℃; precipitation of the co-eutectic $Mg_2Si$ phase started at 581 ℃, and performed parallel to the eutectic reaction $T_{E,Mg2Si}$ = 559.5 ℃; and finally, precipitation of the AlMg-$\beta$ phase at 335 ℃. On the base of equilibrium calculation, the melt was stable in temperature interval 743–522 ℃.

### 3.2. Simultaneous thermal analysis

Applied method of DSC resulted in cooling curve obtained at cooling rate of 0.17 K $s^{-1}$, shown in Fig. 4, together with its first derivation, which enabled determination of the characteristic temperatures.

The DSC cooling curve resulted in exact values of significant temperatures of the phase transformations. Solidification starting temperature (liquidus temperature) at 596.1 ℃, and eutectic evolution temperature at 574.8 ℃ were indicated on the cooling curve. The area below the curve consists of two peaks as indicated by first derivation curve. These peaks indicate eutectic interval of complex multicomponent phase development. Nevertheless, eutectic evolution interval ended at ∼ 530 ℃. The cooling curve also enabled determination of the secondary eutectic evolution at 433.8 ℃.

Frozen microstructure obtained by rapid cooling, comprehending preliminary solidification microstructure obtained before the quenching, proceeded, and forced solidification microstructure formed during the quenching process. A frozen microstructure consists of the particular ratios of preliminary and forcibly solidified phases, dependent on the quenching temperature. The morphology of evaluated phases is also dependent on the quenching temperature. The ratio and morphology of the particular phases, evaluated dependent on the quenching temperature, were determined by microstructural investigations.

Figure 5 shows EDS analysis performed on the sample quenched from the highest temperature.

Microstructural constituents of analyzed microstructure are as follows: grey field of the primary dendrites of $\alpha_{Al}$ aluminum, $Mg_2Si$ polyeders surrounded by characteristic branched black phase $Mg_2Si$ and white intermetallic phase mostly with the Chinese script morphology in the quenched zones. Presumed stoichiometry is $Al_x(Fe,Mn)_ySi_z$, however, the switching of the Si atoms with the Mg atoms occurs probably due to the extreme quenching conditions. The laid grey phase $Al_8Mg_5$ with the irregular morphology has been precipitated interdendritic. In the equilibrium conditions of the cooling and solidification by quenching process application the occurrence of any additional phase has not been noticed, nor the preferred precipitation of particular phase. Frequent precipitation of the $Mg_2Si$ phase with the polyedric morphology can be seen at higher quenching temperatures. Cited occurrence can be attributed to the thermodynamically stable morphologies (approaching to the sphere form) in given conditions.

The grain size and characteristics of developed phases related to the quenching temperature are compared and indicated in Fig. 6. Micrographs are related to samples quenched at temperatures/temperature intervals of the phase transformations: $T_Q > T_L$, $T_Q \sim T_L$, $T_L > T_Q > T_{E1s}$, $T_{E1s} > T_Q > T_{E1e}$, $T_Q > T_{E2}$, where the temperature meanings are: $T_Q$ is quenching temperature (℃), $T_L$ is liquidus temperature (℃), $T_{E1s}$ is temperature of primary eutectic development start (℃), $T_{E1e}$ is temperature of primary eutectic evolution end (℃), $T_{E2}$ is secondary eutectic evolution temperature (℃).

Figure 6a shows microstructure development at highest quenching temperature, $T_Q$ = 606.3 ℃ ($T_Q > T_L$). Microstructural investigations show that some part of preliminary solidification already occurs before the quenching process performing, i.e. clear difference between preliminary developed coarse grains and the quenched zones of fine equiaxed microstructure, marked in the figures, is shown. On the base of microstructure examination by optical microscope, the conclusion could be imposed, related to the weak

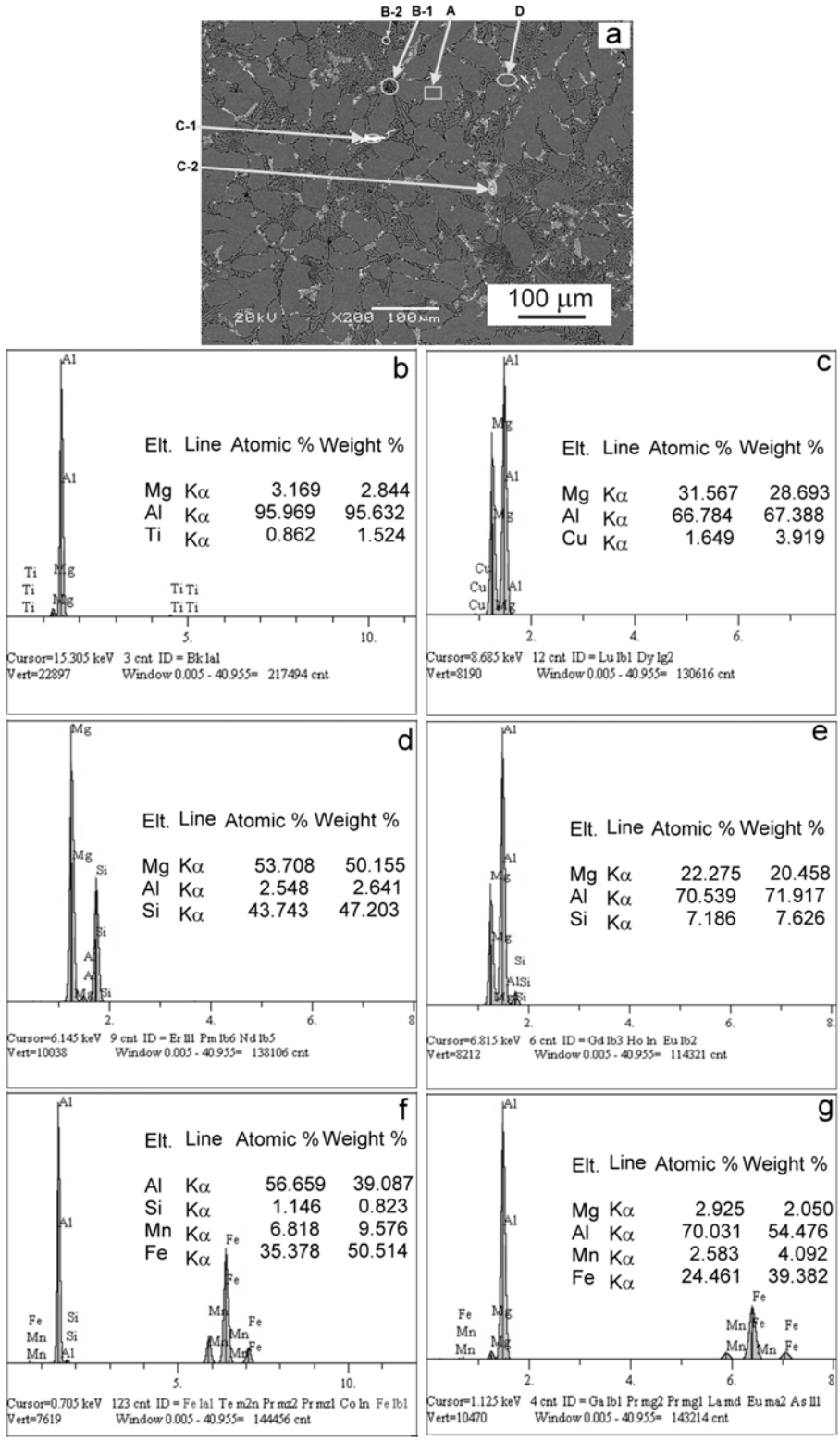


Fig. 5. Qualitative microstructural analysis of the sample quenched at temperature $T_Q = 587.6\,^{\circ}\mathrm{C}$ ($T_L > T_Q > T_{E1s}$): a) SEM micrographs with the marked places of analysis, b) place B-1, black phase, polyeder; Mg, Si; stoichiometry: $Mg_2Si$, c) place B-2, black phase, Mg, Si; stoichiometry: $Mg_2Si$, d) place A, matrix, $\alpha_{Al}$, e) place C-1; white phase – needles, Al, Fe, Mn, Si; stoichiometry: $Al_x(Fe,Mn)_ySi_z$, f) place C-2; white phase – Chinese script, Al, Fe, Mn, Mg; stoichiometry: $Al_x(Fe,Mn)_yMg_z$, g) place D, grey phase, $Al_8Mg_5$.

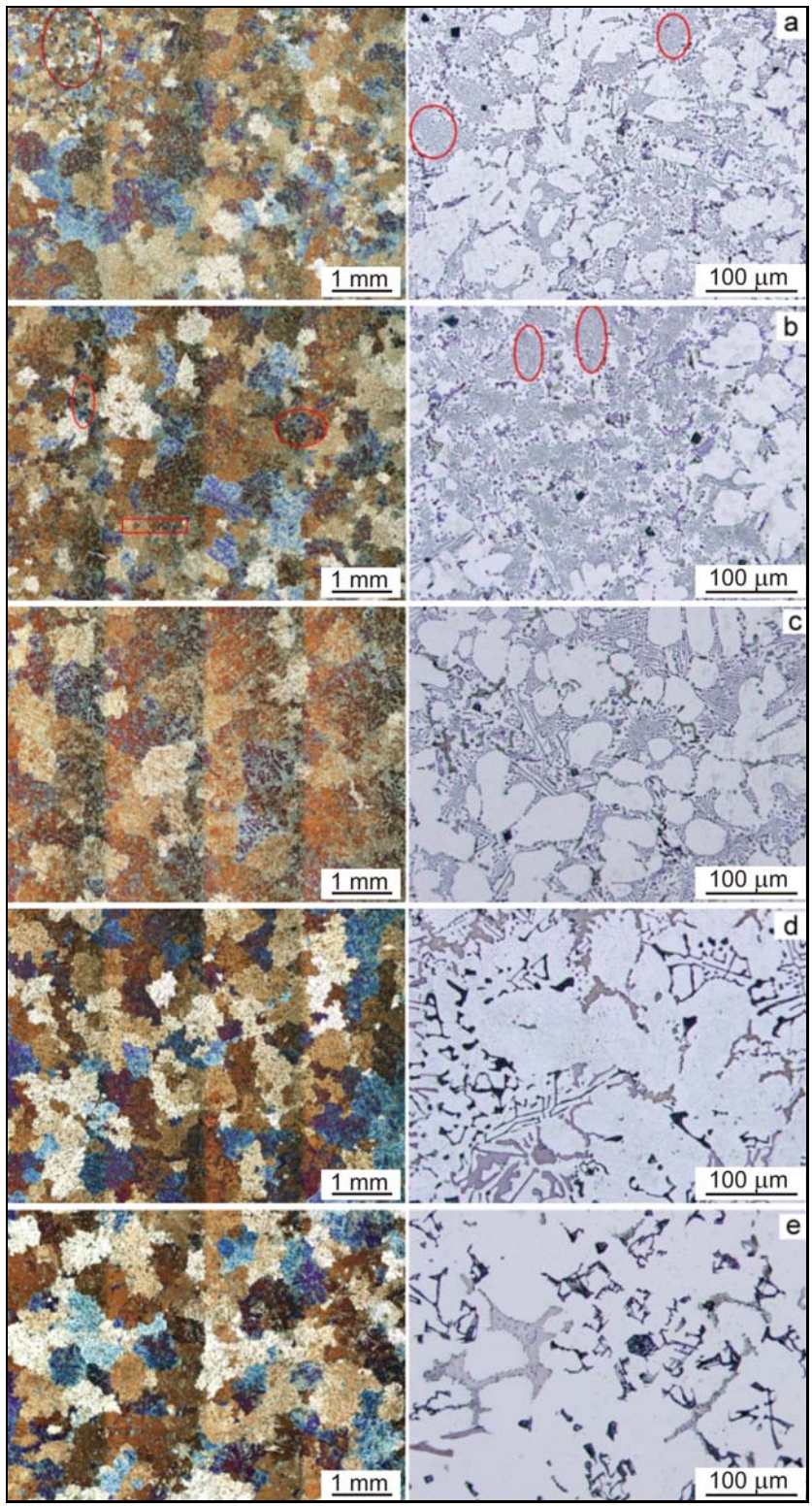


Fig. 6. Comparable overview of electrolytic and metallographic etched microstructure of samples quenched at characteristic temperatures/temperature intervals: a) $T_Q = 606.3\,℃$ ($T_Q > T_L$), b) $T_Q = 594.1\,℃$ ($T_Q \sim T_L$), c) $T_Q = 587.6\,℃$ ($T_L > T_Q > T_{E1s}$), d) $T_Q = 574.9\,℃$ ($T_{E1s} > T_Q > T_{E1e}$), e) $T_Q = 491.3\,℃$ ($T_Q > T_{E2}$).

development of primary dendrites $\alpha_{Al}$ and significant ratio of fine polyeders of $Mg_2Si$ surrounded by branched morphologies of the $Mg_2Si$ eutectic colonies. The development of the $Al_8Mg_5$ phase was noticed on the boundaries of eutectic cells and primary dendrites. The iron phase is very fine and completely in

the Chinese script morphology, due to the high cooling rate.

Figure 6b represents the sample quenched from the temperature close to the liquidus one ($T_Q \sim T_L$). Electrolytically etched microstructure also reveals an existence of zones with finely frozen microstructure obtained by quenching. Very similar microstructure development, as in previous case ($T_Q > T_L$) was noticed with some preliminary evaluated primary dendrites $\alpha_{Al}$ and significant ratio of very fine eutectic $Mg_2Si$ colonies. Development of fine, but compacted $Al_8Mg_5$ phase on the eutectic cells and primary dendrites boundaries continued. The iron phase $Al_x(Fe,Mn)_ySi_z$ still had exclusively fine morphology of Chinese script form.

Quenching from the temperature $T_Q = 587.6$ ℃ ($T_L > T_Q > T_{E1s}$) is shown in Fig. 6c. In this case, the primary dendrites were more intensively expressed, as well as clear difference between preliminary completely developed and quenched eutectic $Mg_2Si$ phase branched around, now much bigger polyeders. The phase $Al_8Mg_5$ is obviously the last one to precipitate on the eutectic cell boundaries as well as in the interdendritic spaces.

Decreasing of the quenching temperature enables a longer time for performing of preliminary solidification (Figs. 6d,e). Generally, the successive increase of the size of the microstructural constituents, as well as the size of the primary dendrites of $\alpha_{Al}$ with the decrease of the quenching temperature occurred. The following quenching processes conditioned total eutectic $Mg_2Si$ development with branched morphology growing around coarse polyeders. The iron phases show a tendency to the needle morphology precipitation. Big compacted particles of the $Al_8Mg_5$ phase surround the primary dendrites. It can be noticed that $Al_8Mg_5$ phase becomes more serrated with decrease of quenching temperature, i.e. slower cooling and enough time for development of $\alpha_{Al}$ in cellular mode.

Temperature intervals and kinetic of particular phases evolution have been determined on the base of phase analysis of quenched samples related to the quenching temperature, as shown in Fig. 7.

The stability of the $Al_x(Fe,Mn)_ySi_z$ phase was established at above calculated liquidus temperature $T_L = 597.3$ ℃ and the biggest development intensity was noticed in the temperature interval 582.9–569.9 ℃, when it achieves intermetallic phase ratio of 0.71 after 119.3 s, afterwards a small increase of the ratio to the maximum 0.78 occurs.

The phase $Mg_2Si$ expectedly begins to evaluate as a co-eutectic phase at 582.0 ℃ after 38.5 s. Ratio of this phase stays approximately constant after 541.9 ℃ and 270 s. Maximum value of the phase ratio was 0.83.

Precipitation of the $Al_8Mg_5$ phase did not occur in the solid state. This phase developed as a low temperature secondary eutectic. In Fig. 8 the evidence of its presence was noticed even at high temperatures in significant ratio of $f\ (Al_8Mg_5) = 0.20$ due to the non-equilibrium conditions and forced solidification. It seems that its precipitation occurred soon after primary dendrites evolution and eutectic colony development, but afterwards it was repressed to the interdendritic spaces. Regarding to compact morphology, calculation of its surface area reached high values. Very briefly this phase achieved high ratio of $f(Al_8Mg_5) = 0.8911$ even at 565.5 ℃, after only 121.7 s after pouring, and maximum value of its ratio was 0.9692.

Mathematical expressions of the temperature and time evolution of particular phases were made:

| | | |
|---|---|---|
| *f*-$T_Q$ | $f\ (Al_x(Fe,Mn)_ySi_z) = 0.04 + (0.72 - 0.04)/(1 + \exp((T_Q - 577.15)/1.45))$ | $R^2 = 0.95$ |
| *f*-*t* | $f(Al_x(Fe,Mn)_ySi_z) = 0.73 + (-0.05 - 0.73)/(1 + \exp((t - 83.09)/20.06))$ | $R^2 = 0.99$ |
| *f*-$T_Q$ | $f(Mg_2Si) = -0.006 + (0.74 + 0.006)/(1 + \exp((T_Q - 574.23)/5.07))$ | $R^2 = 0.95$ |
| *f*-*t* | $f(Mg_2Si) = 0.74 + (-0.18 - 0.74)/(1 + \exp((t - 93.20)/50.52))$ | $R^2 = 0.97$ |
| *f*-$T_Q$ | $f(Al_8Mg_5) = -1.17 \times 10^{-12} \exp(T_Q/22.87) - 1.19 \times 10^{-12} \exp(T_Q/22.87) - -1.17 \times 10^{-12} \exp(T_Q/22.87) + 0.97$ | $R^2 = 0.89$ |
| *f*-*t* | $f(Al_8Mg_5) = -0.59 \exp(-t/56.56) - 0.59 \exp(-t/56.56) + 0.91$ | $R^2 = 0.91$ |

Performed phase analysis of the samples quenched from the different temperatures resulted in the following ratios of particular phases in microstructure as given in Fig. 8.

Ratios of the $Al_x(Fe,Mn)_ySi_z$ and $Mg_2Si$ phases show decreasing trend with the lowering of the cooling intensity, i.e. quenching temperature. The phase $Al_x(Fe,Mn)_ySi_z$ at the lower quenching temperatures ($T_Q < T_E$) concisely keeps its ratio in the interval 1.75–2.50 area %, while the $Mg_2Si$ phase ratio in the same temperature interval stays constant around 5–6 area %. The phase $Al_8Mg_5$ shows oscillating behavior by the following of Boltzmann curve, but its ratio below $T_E$ was in interval of 2–3 area %. The content of the $Al_8Mg_5$ phase increases in the temperature interval from 587.6–574.9 ℃ when it achieves its final ratio of ∼ 3 area % which it keeps to the end of solidification. The final temperature of the $Al_8Mg_5$ phase maximum ratio of evolution was 574.9 ℃ which corresponded to the thermodynamic data from the cooling curves related to the secondary eutectic precipitation. Since it was precipitating at rather high temperat-

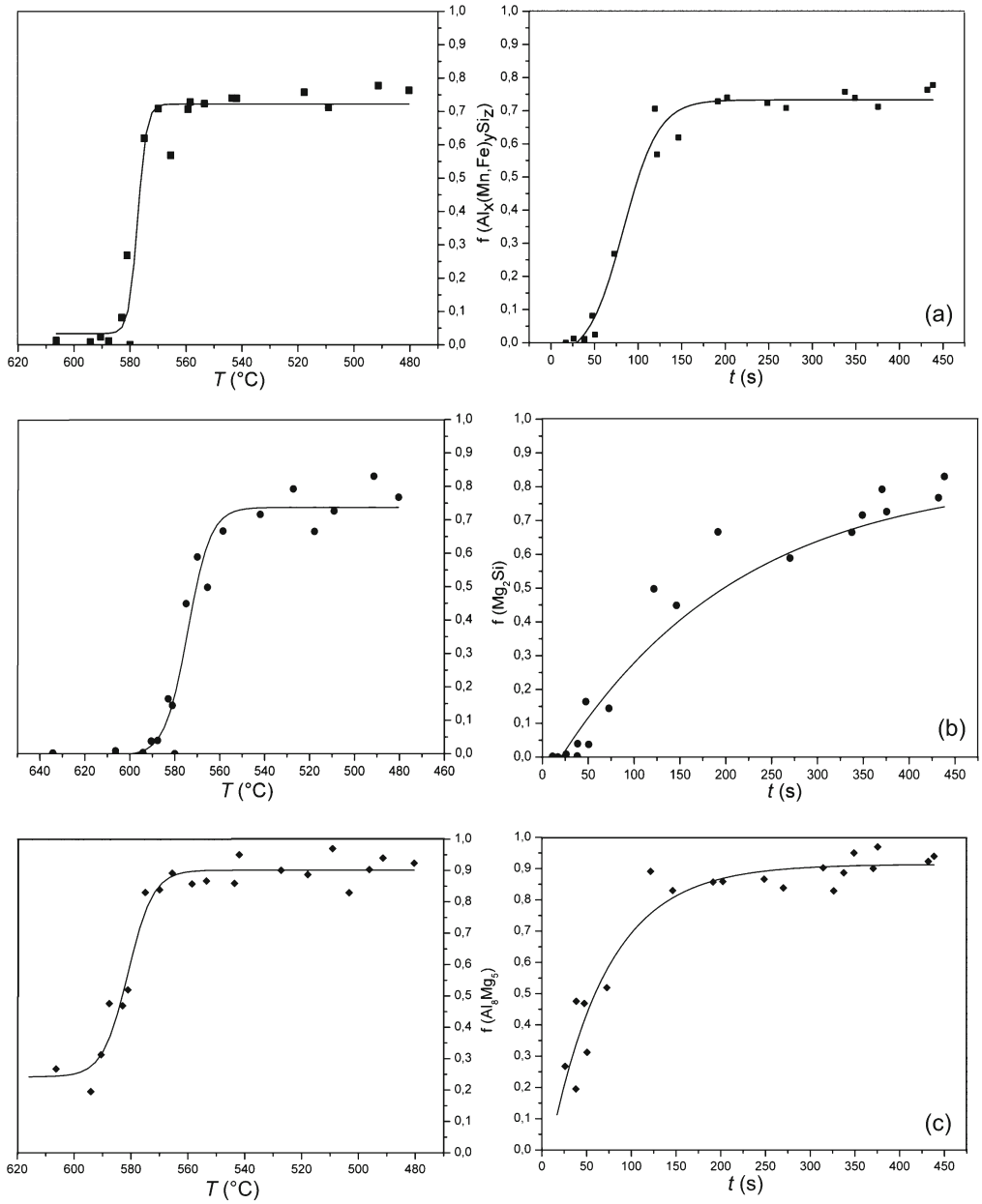


Fig. 7. Temperature and time dependent evolution of following phases: a) $Al_x(Fe,Mn)_ySi_z$, b) $Mg_2Si$ and c) $Al_8Mg_5$.

ures, immediately after the co-eutectic $Mg_2Si$ phase development, the repressing to the cells boundaries and interdendritic spaces occured. Mathematical expressions of behavior of the particular phase ratios in dependence on the quenching temperature were made:

$$f(Al_x(Fe,Mn)_ySi_z) = -9.56\exp(-T_Q/164.30) - 9.56\exp(-T_Q/164.30) - 9.56\exp(-T_Q/164.30) + 3.48$$

$$f(Mg_2Si) = -17.71\exp(-T_Q/320.28) - 17.71\exp(-T_Q/320.28) - 17.71\exp(-T_Q/320.28) + 16.59$$

$$f(Al_8Mg_5) = 1.12 + (2.83 - 1.12)/(1 + \exp((-T_Q - 584.11)/4.20))$$

## 4. Conclusions

On the base of AlMg9 alloy investigations by simultaneous thermal analyses and analysis of microstructural characteristics by application of "disturbed" solidification method, the solidification sequence was established. Besides this, the following conclusions were determined:

– Thermodynamic calculation of the equilibrium stability of particular phases by ThermoCalc resulted in presumed solidification sequence: $Al_{13}Fe_4$, $Al_6Mn$, $\alpha_{Al}$, $Mg_2Si$ and finally AlMg-$\beta$. The melt is on the base of equilibrium calculation stable in limited temperature interval of 743–522 ℃.

– Microstructural constituents in samples quen-

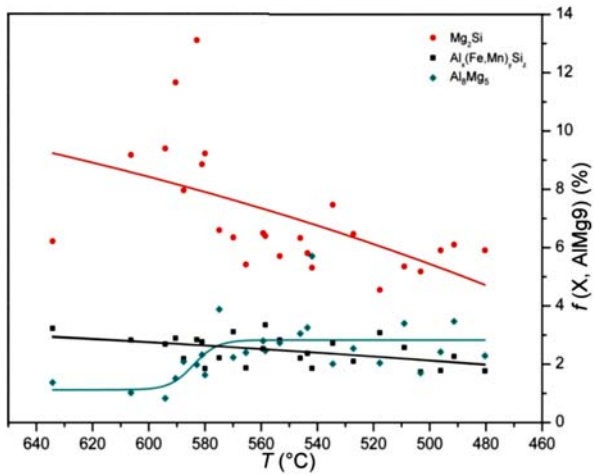


Fig. 8. Ratio of particular phases in microstructure: $Al_x(Fe,Mn)_ySi_z$, $Mg_2Si$ and $Al_8Mg_5$.

ched at all temperatures established by EDS were: $Al_x(Fe,Mn)_ySi_z$, either the Chinese script or needle-like morphology, $Mg_2Si$, with the polyeder morphology surrounded by branched eutectic, and $Al_8Mg_5$ phase of compacted irregular shape, but relatively big particles precipitated as a second eutectic phase. Phases $Al_{13}Fe_4$, $Al_6Mn$ established by thermodynamic modeling were not determined in investigated microstructures due to later $Al_x(Fe,Mn)_ySi_z$ formation, as well as AlMg-$\beta$, which was evaluated as $Al_8Mg_5$ phase.

– Simultaneous thermal analysis (DSC technique) enabled significant temperatures of the phase transformations establishing: $T_L = 596.1\,℃$; temperature of the eutectic development starts $T_{E1} = 574.8\,℃$, and temperature of the secondary eutectic phase evolution $T_{E2} = 433.8\,℃$.

– By the "disturbed" solidification method complete temperature and time interval of solidification have been covered. An analysis of the microstructural characteristics of particular phases resulted in mathematical expression of temperature and time intervals of evolution of particular phases in next solidification sequence (Table 3).

– Phase analysis related to the quenching temperature, i.e. cooling intensity, resulted in mild decreasing trend of the $Al_x(Fe,Mn)_ySi_z$ ratio, and noticed decrease of $Mg_2Si$ phase ratio, while the $Al_8Mg_5$ phase grew with decrease of the quenching temperature to the $\sim 540\,℃$, below which it kept its value constant.

Investigations of multicomponent technical AlMg9 alloy resulted in the qualitative and quantitative description of the solidification sequence at corresponding temperature and time intervals. The solidification sequence enabled stability prediction of required or suitable phases, and therefore provided the parameters for the solidification process to obtain required microstructural characteristics.

## References

[1] KARLÍK, M.—SLÁMOVÁ, M.—MANÍK, T.: Kovove Mater., *49*, 2009, p. 139.
[2] USTA, M.—EKMEKÇILER, E.: Kovove Mater., *48*, 2010, p. 249. doi:10.4149/km_2010_4_249
[3] MICHALCOVÁ, A.—VOJTĚCH, D.—SCHUMACHER, G.—NOVÁK, P.—KLEMENTOVÁ, M.—ŠERÁK, J.—MUDROVÁ, M.—VALDAUFOVÁ, J.: Kovove Mater., *48*, 2010, p. 1. doi:10.4149/km_2010_1_1
[4] ZOVKO BRODARAC, Z.—MRVAR, P.—MEDVED, J.: Kovove Mater., *47*, 2009, p. 209.
[5] MURRAY, J. L.: Al-Mg (Aluminum-Magnesium). In: Binary system of aluminum – admixture and their importance for metallurgy. Eds.: Kuchař, L., Drápala, J. Ostrava, Vysoká škola báňská – Technická univerzita Ostrava 2003, p. 82.
[6] ASM Handbook®. Vol. 3. Alloy Phase Diagrams. Ed.: Baker, H. Materials Park, Ohio 1992.
[7] MONDOLFO, L. F.: Aluminum Alloys, Structure and Properties. London, Butterworths 1976.
[8] SCHUMANN, H.: Metallographie. Leipzig, VEB Deutscher Verlag für Grundstoffindustrie 1975.
[9] BELOV, N. A.—ESKIN, D. G.—AKSENOV, A. A.: Multicomponent Phase Diagrams: Applications for Commercial Aluminum Alloys. London, Elsevier 2005.
[10] FILETIN, T.—KOVAČIČEK, F.—INDOF, J.: Properties and application of materials. Zagreb, University of Zagreb, Faculty of the Mechanical Engineering and Naval Architecture 2002, p. 143.
[11] LIU, Y. L.—KANG, S. B.: Materials Science and Technology, *13*, 1997, p. 331.
[12] WARMUZEK, M.: Metallography and Microstructure of non ferrous Alloys, Metallographic Techniques for Aluminum and its Alloys. ASM Handbook®, Vol. 9, Metallography and Microstructures, ASM International, Ohio 2004.
[13] EN 1706: 1998, Aluminum and aluminum alloys – Castings – Chemical composition and mechanical properties.

Table 3. The analysis of the microstructural characteristics of particular phases

| Reaction No. | Reaction | Registered temperature | Temperature of the reaction performing on the base of experimentally obtained data (℃) |
|---|---|---|---|
| 1 | $L \rightarrow L' + Al_x(Fe,Mn)_ySi_z$ | $T_N$ | $< 627.0$ |
| 2 | $L' \rightarrow L'' + \alpha_{Al}$ | $T_L$ | 602.7–586.8 |
| 3 | $L'' \rightarrow L''' + (\alpha_{Al} + Mg_2Si)$ | $T_{E1}$ | 586.8–515.4 |
| 4 | $L''' \rightarrow \alpha_{Al} + Al_8Mg_5$ | $T_{E2}$ | 442.1–421.7 |